# Discovery of Chiral Cyclopropyl Dihydro-Alkylthio-Benzyl-Oxopyrimidine (*S*-DABO) Derivatives as Potent HIV-1 Reverse Transcriptase Inhibitors with High Activity Against Clinically Relevant Mutants

Marco Radi,[†,‡] Giovanni Maga,[†,§] Maddalena Alongi,[‡] Lucilla Angeli,[‡] Alberta Samuele,[§] Samantha Zanoli,[§] Luca Bellucci,[‡] Andrea Tafi,[‡] Gianni Casaluce,[‡] Gianluca Giorgi,[∥] Mercedes Armand-Ugon,[⊥] Emmanuel Gonzalez,[⊥] José A. Esté,[§] Mireille Baltzinger,[▽] Guillaume Bec,[#] Philippe Dumas,[#] Eric Ennifar,[#] and Maurizio Botta*[,‡]

*Dipartimento Farmaco Chimico Tecnologico, University of Siena, Via Alcide de Gasperi 2, I-53100 Siena, Italy, Istituto di Genetica Molecolare, IGM-CNR, Via Abbiategrasso 207, I-27100 Pavia, Italy, Dipartimento di Chimica, University of Siena, Via Alcide de Gasperi 2, I-53100 Siena, Italy, Retrovirology Laboratory irsiCaixa, Hospital Universitari Germans Trias i Pujol, Universitat Autònoma de Barcelona, E-08916 Badalona, Spain, Architecture et Réactivité de l'ARN, UPR 9002 CNRS/Université Louis Pasteur, 15 rue René Descartes, 67084 Strasbourg, France, UMR 7175 CNRS/Université Louis Pasteur, Ecole Supérieure de Biotechnologie Strasbourg, Boulevard Sébastien Brandt, F-67400 Illkirch, France*

*Received October 21, 2008*

The role played by stereochemistry in the C2-substituent (left part) on the *S*-DABO scaffold for anti-HIV-1 activity has been investigated for the first time. A series of *S*-DABO analogues, where the double bond in the C2-substituent is replaced by an enantiopure isosteric cyclopropyl moiety, has been synthesized, leading to the identification of a potent lead compound endowed with picomolar activity against RT (wt) and nanomolar activity against selected drug-resistant mutants. Molecular modeling calculation, enzymatic studies, and surface plasmon resonance experiments allowed us to rationalize the biological behavior of the synthesized compounds, which act as mixed-type inhibitors of HIV-1 RT K103N, with a preferential association to the enzyme−substrate complex. Taken together, our data show that the right combination of stereochemistry on the left and right parts (C6-substituent) of the *S*-DABO scaffold plays a key role in the inhibition of both wild-type and drug-resistant enzymes, especially the K103N mutant.

## Introduction

The drug arsenal for the war on AIDS currently comprises 25 approved drugs belonging to six different classes of anti-HIV inhibitors[1] that target viral enzymes and proteins. The only exception is Maraviroc (UK-427,857),[2] which targets a cellular cofactor (CCR5). The development of drugs that are active against different targets represents an important step forward in the eradication of HIV, especially drug-resistant mutations. However, recent clinical studies demonstrated that therapies based on Maraviroc and Raltegravir have comparable efficacy to regimens based on the non-nucleoside reverse transcriptase inhibitor (NNRTI[a]) Efavirenz.[3] Reverse transcriptase (RT) therefore represents an old but still important target for the identification of novel NNRTIs endowed with a better activity profile against clinically relevant mutant strains.[4] Non-nucleoside reverse transcriptase inhibitors include more than 30 structurally different classes of molecules such as Nevirapine, TIBO, DABO, HEPT, TNK-651, ITU, DATA and DAPY (Chart 1).[5] Among the NNRTIs reported to date, the members of the DABO family (namely *S*-DABOs, DABOs, *NH*-DABOs, $F_2$-*N*,*N*-DABOs, DATNOs) present a very similar binding mode within the non-nucleoside inhibitor binding pocket (NNBP) characterized by a key hydrogen-bond contact between the NH at position 3 of the pyrimidinone and Lys101 (Figure 1, zone C).[6] In addition, C5 and C6 substituents establish important hydrophobic interactions with a large pocket defined by the residues of zone A and

**Chart 1.** Structure of Common NNRTIs

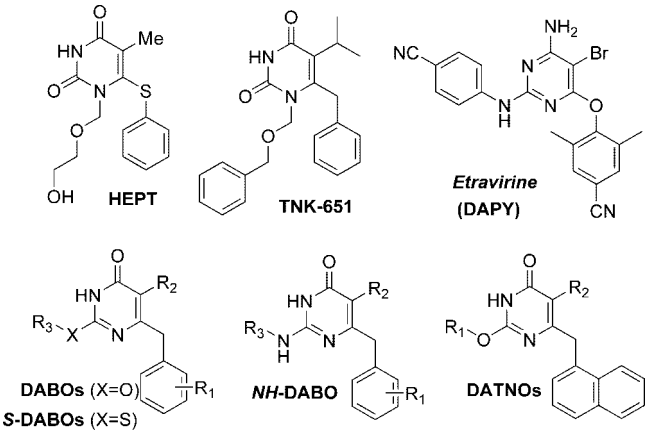


* To whom correspondence should be addressed. Phone: (+39)0577-234306. Fax: (+39)0577-234333. E-mail: botta@unisi.it.
† These authors equally contributed to this work.
‡ Dipartimento Farmaco Chimico Tecnologico, University of Siena.
§ Istituto di Genetica Molecolare, IGM-CNR.
⊥ Retrovirology Laboratory irsiCaixa, Hospital Universitari Germans Trias i Pujol, Universitat Autònoma de Barcelona.
∥ Dipartimento di Chimica, University of Siena.
▽ UMR 7175 CNRS/Université Louis Pasteur, Ecole Supérieure de Biotechnologie Strasbourg.
# Architecture et réactivité de l'ARN, UPR 9002 CNRS/Université Louis Pasteur.

[a] Abbreviations: *S*-DABO, dihydro-alkylthio-benzyl-oxopyrimidines; HIV-1, human immunodeficiency virus type-1; WT, wild type; NNRTIs, nonnucleoside reverse transcriptase inhibitors; DABOs, dihydro-alkyloxy-benzyl-oxopyrimidines; DATNOs, dihydroalkylthio-naphthylmethyl-oxopyrimidines; EFV, efavirenz; $F_2$-*N*,*N*-DABOs, 5-alkyl-2-(*N*,*N*-disubstituted)amino-6-(2,6-difluorophenylalkyl) pyrimidin-4(3*H*)ones; HEPT, 1-[(2-hydroxyethoxy)methyl]-6-(phenylthio)thymine; *NH*-DABOs, dihydro-alkylamino-benzyl-oxopyrimidines; NVP, nevirapine; TIBO, tetrahydroimidazo[4,5,1-*jk*][1,4]benzodiazepinone; DAPY, diarylpyrimidine; DATA, diaryltriazine; ITU, imidoylthiourea; SAR, structure−activity relationship; NNBP, non-nucleoside binding pocket; PDB, protein data bank; MD, molecular dynamics; rmsd, root-mean-square deviation; PBC, periodic boundary conditions; PME, particle-mesh-Ewald; NPT, number of molecules pressure and temperature; SPR, surface plasmon resonance; NA, nucleic acid; dNTP, deoxyribonucleotide triphosphate.

10.1021/jm801330n CCC: $40.75 © 2009 American Chemical Society
Published on Web 01/13/2009

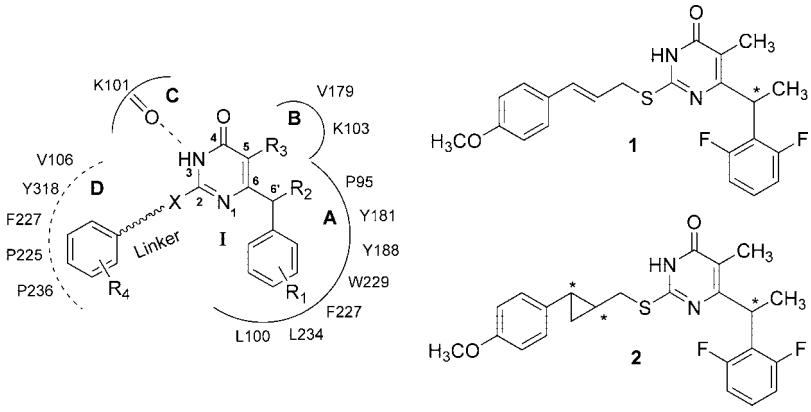


**Figure 1.** Interactions of a generic C2-arylalkyl *S*-DABO (**I**) within the NNBP and structures of compound **1** and target analogue **2**.

B depicted in Figure 1. The substituent at position C2, which is characteristic for each DABO family, establishes a series of interactions within the NNBP for which a clear structure−activity relationship (SAR) has not been established yet.

During the course of a study aimed at exploring the relationship between the C2-functionalization of the *S*-DABO scaffold and the anti-HIV activity, our research group first reported how the introduction of an arylalkyl moiety in C2 significantly increased the antiviral activity due to profitable hydrophobic interaction with a large pocket (zone D) of the allosteric site.[7] Subsequent molecular dynamics studies showed that the right combination of the C2 linker length and the $R_4$ substituent on the phenyl ring played a key role in the opening of the NNBP of the K103N mutant.[8] Compound **1** (Figure 1) emerged as the most interesting inhibitor for its activity on MT-4 cells infected with both HIV-1 wild type (NL-43 wt) and clinically relevant mutants, especially the one bearing the K103N mutation. In the search for new C2-substituted *S*-DABO analogues, Nawrozkij et al. have recently reported the synthesis and biological investigation of many C2-arylalkyl *S*-DABO analogues. Among them, the only interesting compounds were represented by the C2-oxophenethyl derivatives. However, these showed low antiviral potency against clinically relevant drug-resistant mutants.[9] It is well-known that, to identify high quality lead compounds, it is important to address the relationship between drug-chirality and activity early in the drug discovery process.[10] From this point of view, while the role played by the stereochemistry in the right part of the *S*-DABO scaffold for the activity on RT (wt) has already been established,[11] no reports have been published so far on the role played by the stereochemistry of the left part of the molecule.

Considering the importance of the C2 substituent of **1** for the antiviral activity, we decided to introduce a chiral moiety on the left part of the molecule **1**, trying not to disrupt the topology/flexibility of the parent compound. Accordingly, we planned to convert compound **1** into its cyclopropyl bioisoster **2**: the cyclopropyl moiety would not only allow us to introduce two new stereocenters while maintaining the optimal length of the C2-linker but it is also a bulky lipophilic substituent that could give additional interactions with the hydrophobic residues of zone D. Furthermore, as described in our previous simulations on the K103N mutant,[8] the side chains of residues Lys101 and Val179 shaped a sort of crevice on the external surface of the closed enzyme. This hydrophobic area lies in close proximity to the C2-linker and could therefore be exploited by the lipophilic cyclopropyl group, giving an additional contribution to the generation of the allosteric binding pocket. In addition, the introduction of different stereocenters on important pharmacophoric sites of a promising RT-inhibitor such as **1** could allow us to generate a collection of enantiopure drugs with improved activity and potentially usefulness in overcoming future drug-induced mutations.

## Result and Discussion

The synthesis of the title compounds (Scheme 1) started with the reduction of the commercially available *p*-methoxy cinnamaldehyde **3** with $NaBH_4$ to give the cinnamyl alcohol **4**. The cyclopropane ring was then built on the double bond using the Furukawa reagent (diethyl zinc and diiodomethane) alone[12] or in the presence of a chiral promoter (1,2-bis(methanesulfonylamino)cyclohexane)[13] to give *rac*-**5**, (*S*,*S*)-**5**, and (*R*,*R*)-**5**, respectively (Scheme 1). The last two compounds were obtained in 98% ee as determined by high-performance liquid chromatography (HPLC) on Chiralcel OD column (see Experimental Section for details). The racemic and enantiopure cyclopropyl derivatives **5** were then coupled with 6-(1-(2,6-difluorophenyl)-ethyl)-5-methyl-3,4-dihydro-2-thioxopyrimidin-4(3*H*)-one via a microwave-assisted Mitsunobu reaction to give the *S*-DABO derivatives *rac*-**2**, **2a**, and **2b**.

The diastereoisomeric mixtures **2a** and **2b** were finally resolved by semipreparative HPLC on ALLTIMA C18 column thus obtaining each single diasteroisomer (**2c**−**f**) with high diasteromeric excess (>98%) (see Experimental Section for details). The absolute stereochemistry of the four isomers was determined by X-ray crystallography of **2d** (*R*,*R*,*S*),[14] which showed four crystallographic independent molecules constituting the asymmetric unit of **2d** (see Supporting Information). Each molecule shows a "folded" conformation with the difluorophenyl moiety pointing toward the methoxyphenyl ring while the latter is almost perpendicular to the cyclopropane with a dihedral angle that means 83.8(7)° in the four molecules (Figure 2).

The pure compounds **2c**−**f** were then submitted to biological evaluation in cell-free assay using Nevirapine and Efavirenz as reference compounds. As reported in Table 1, the results of the biological screening clearly highlighted the importance of the right combination of stereochemistry on the left and right part of the *S*-DABO scaffold for the inhibition of both RT(wt) and drug resistant mutants (especially the K103N). Comparing the activity data of compounds **2c** and **2f**, it was clear that the (*R*,*R*) configuration of the cyclopropane was fundamental for the better activity profile of **2c** against the clinically relevant K103N drug resistant mutant. This consideration was further reinforced by the biological evaluation of the two enantiomers of compound **1** obtained via semipreparative HPLC resolution (see Experimental Section for details) and for which absolute configuration was determined by converting them into the known compounds

**Scheme 1**[a]

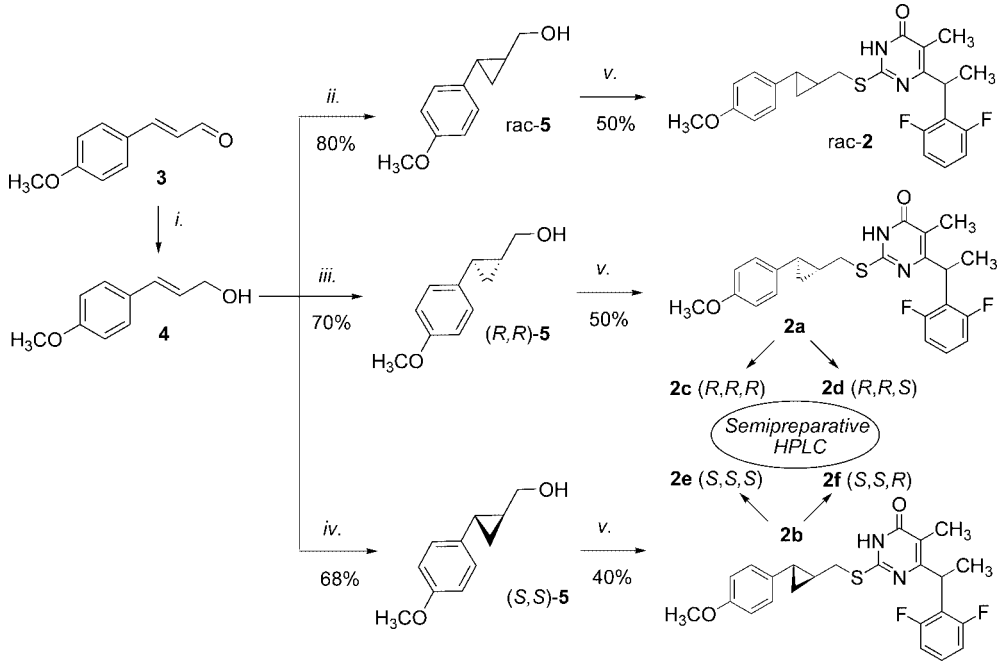


[a] (i) $NaBH_4$, MeOH, rt, 1h; (ii) $Et_2Zn$, $CH_2I_2$, 0 °C. (iii) (a) (*R*,*R*)-1,2-bis(methanesulfonylamino)cyclohexane, $Et_2Zn$, $ZnI_2$; (b) $Et_2Zn$, $CH_2I_2$. (iv) (a) (*S*,*S*)-1,2-bis(methanesulfonylamino)cyclohexane, $Et_2Zn$, $ZnI_2$; (b) $Et_2Zn$, $CH_2I_2$; (v) 6-(1-(2,6-difluorophenyl)-ethyl)-5-methyl-3,4-dihydro-2-thioxopyrimidin-4(3*H*)-one, $(CH_3)_3P$, DIAD, DMF, MW 40 °C, 10 min.

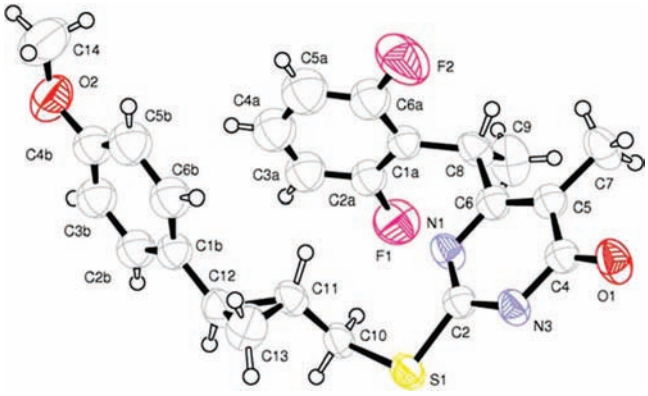


**Figure 2.** X-ray crystal structure of **2d**. Only one of the four molecules constituting the asymmetric unit is reported. Ellipsoids enclose 50% probability.

**Table 1.** Anti-HIV-1 Activity of Compounds **1**−**2** in Cell Free Assay

| | $ID_{50}$ ($\mu$M)[a,b] | | |
|---|---|---|---|
| compd | wt | K103N | Y181I |
| *rac*-**2** | 0.04 | 3.00 | 6.00 |
| **2c** (*R*,*R*,*R*) | 0.02 | 0.04 | 0.80 |
| **2d** (*R*,*R*,*S*) | 0.30 | 0.60 | 6.00 |
| **2e** (*S*,*S*,*S*) | 0.12 | 0.83 | 2.30 |
| **2f** (*S*,*S*,*R*) | 0.04 | 0.40 | 0.90 |
| **1** (*S*) | 0.60 | 7.01 | 27.83 |
| **1** (*R*) | 0.01 | 0.47 | 2.99 |
| Nevirapine | 0.40 | 8.00 | 20.00 |
| Efavirenz | 0.04 | 0.40 | 0.10 |

[a] Data represent mean values of at least two experiments; [b] ID50: inhibiting dose 50 or needed dose to inhibit 50% of the enzyme.

**2c** and **2d** via enantioselective cyclopropanation.[15] Compound **1**(*R*) was in fact 10-fold more active than **1**(*S*) both against RT (wt) and mutants but 10-fold less active than **2c** against K103N and Y181I: the presence of a (*R*,*R*) cyclopropyl moiety on the left part of the molecule coupled with a C6′-(*R*)methyl group (as in compound **2c**) determined a marked increase in the inhibitory activity. The pure diasteroisomers **2c**−**f** were finally evaluated on MT-4 cells for their cytotoxicity and anti-HIV activity in comparison with Nevirapine and Efavirenz, used as reference drugs (Table 2). Compound **2c** emerged as the most active *S*-DABO derivative reported so far with a picomolar activity against RT (wt), nanomolar activity against all the tested mutants, and an antiviral profile better than that of Nevirapine and Efavirenz. Taken together, these biological results confirm our previous findings on the SAR for the *S*-DABO inhibitors: while the right part of the molecule seems to modulate the activity against the Y181C and Y188L mutants, the left part seems to play a key role for the activity on the K103N mutant.[8]

**Table 2.** Anti-HIV-1 Activity of Compounds **2c**−**f** in MT-4 Cells

| | $EC_{50}$ ($\mu$M)[a,b] | | | | |
|---|---|---|---|---|---|
| compd | NL4-3 wt | K103N | Y181C | Y188L | $CC_{50}$[c] |
| *rac*-**2** | 0.0006 | 0.52 | 0.16 | 0.045 | 37.3 |
| **2c** (*R*,*R*,*R*) | 0.00007 | 0.036 | 0.013 | 0.0015 | 14.64 |
| **2d** (*R*,*R*,*S*) | 0.0049 | 2.55 | 0.52 | 0.19 | 47.17 |
| **2e** (*S*,*S*,*S*) | 0.090 | 5.51 | 7.24 | 1.08 | >56.25 |
| **2f** (*S*,*S*,*R*) | 0.010 | 3.71 | 2.70 | 0.70 | >56.25 |
| Nevirapine | 0.08 | 3.9 | >7..5 | >7.5 | >7.5 |
| Efavirenz | 0.001 | 0.057 | 0.008 | 0.003 | >0.32 |

[a] Data represent mean values of at least two experiments; [b] EC50:effective concentration 50 or needed concentration to inhibit 50% HIV-induced cell death, evaluated with MTT method in MT-4 cells. [c] CC50: cytotoxic concentration 50 or needed concentration to induce 50% death of noninfected cells.

**Molecular Modeling Calculations.** In the attempt to rationalize the biological data obtained for compounds **2c**−**f**, molecular docking simulations (using Autodock 3.0)[16] were initially performed on RT wild type (PDB entry 1RT2)[17] following a computational protocol previously described by us.[8] The docking simulations clearly showed that only the inhibitors **2c** and **2f** bind the NNBP in the *S*-DABOs' "canonical" way:[7a] two hydrogen bonds between the amide moiety of the pyrimidinone ring and the backbone of Lys101 and an additional H-bond with protonated N atom of Lys101 side-chain, hydro-

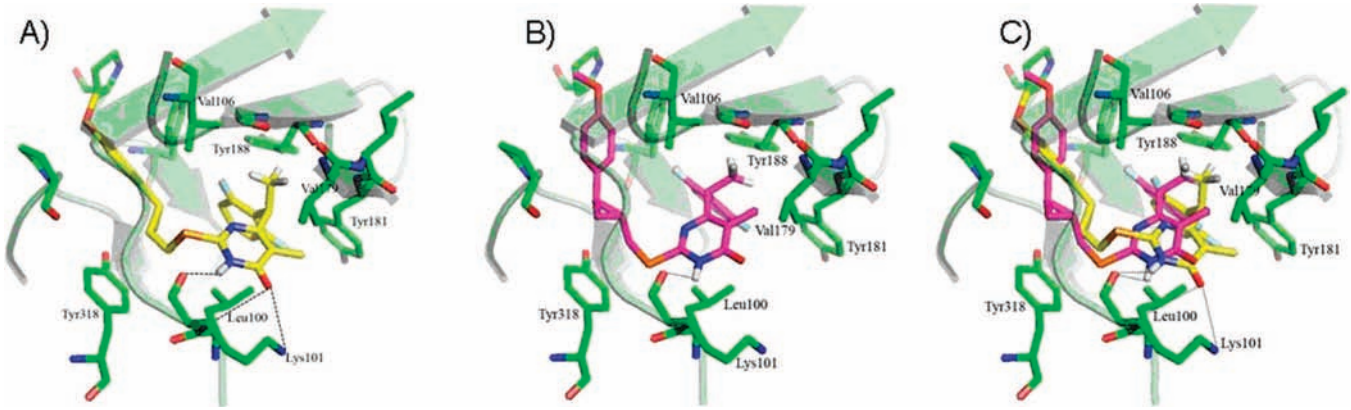


**Figure 3.** (A) Binding mode of compound **2c** (carbon atoms in yellow) as found by docking simulations into the NNBP; compound **2f** shows the same binding mode. (B) Compound **2d** (carbon atoms in purple) as found by docking simulations into the NNBP; compound **2e** shows the same binding mode. (C) Both compounds **2c** and **2d** in the allosteric site.

phobic interactions of the C6-benzyl group with the aromatic cage formed by Tyr181, Tyr188, Phe227, and Trp229 (accessory interactions also with Leu100 and Leu234), and finally very profitable lipophilic interactions between the C6′-(*R*)methyl group and a hydrophobic pocket defined by Val106, Tyr181, Tyr188, Val189, and Gly190 (Figure 3A). On the contrary, compounds **2d** and **2e**, showed a deep modification of the "canonical" binding mode in order to allow the C6′-(*S*)methyl group to establish the above-mentioned hydrophobic interactions. The pyrimidinone ring tilts and loses the hydrogen bond with *N*-amidic of Lys101 backbone, while the benzyl ring, shifting toward Tyr188, loses favorable contacts with the aromatic ring of Tyr181 (Figure 3B,C).

To confirm the importance of the C6′-methyl group for the lipophilic interactions within the NNBP, Grid[18] maps were calculated for $CH_3$ group (C3 probe) to evaluate the regions of best interaction between this group and the macromolecule. The most favorable minimum point (minimum 1) was located in the lipophilic pocket defined by Val106, Tyr181, Tyr188, Val189, and Gly190, while another one was found between Leu100, Val179, and Tyr181 (minimum 2). The docking calculations clearly demonstrated the importance of mapping the minimum 1 because, among all the first ranked docked conformations of **2c**−**f**, a methyl group fits this minimum. The two methyl groups in C5 and C6′ of compounds **2c** and **2f** exactly mapped minima 1 and 2, while compounds **2d** and **2f** are forced to rearrange within the binding site in order to map minimum 1, losing some other important interactions inside the NNBP (Figure 4).

Although our docking calculations allowed us to rationalize the activity profile of compound **2c**−**f** against RT wild type, these experiments did not give any useful information on the role played by chirality of the left part of the molecule: in fact, the cyclopropyl moiety of the docked inhibitors **2c**−**f** showed comparable interaction within the NNBP.

A striking feature of RT is its considerable conformational flexibility. This has complicated the traditional structure-based drug design approach for the discovery of novel NNRTIs. To overcome this problem, the inclusion of structural variability in a docking study and the concept of ligand-induced fit have been taken into account.[19]

Accordingly, a cross-docking approach (the process of docking each ligand into the binding pocket of a series of different ligand−receptor complexes), followed by a molecular dynamics protocol, were applied to further investigate the role played by the C2 side chain in the antiviral activity.[20]

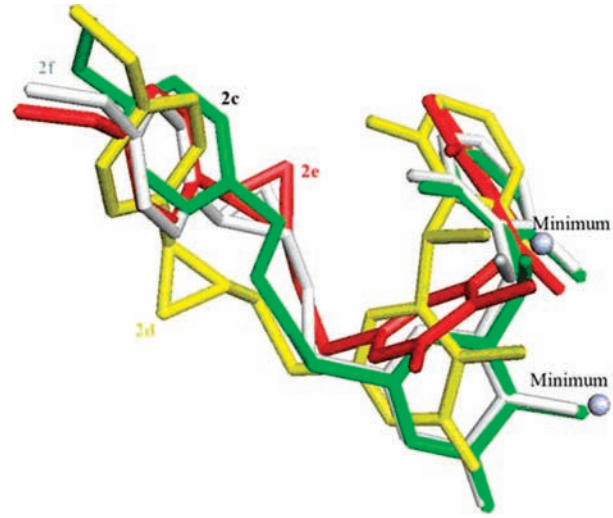


**Figure 4.** Superposition of the lower energy docked conformation of compounds **2c** (green), **2d** (yellow), **2e** (red), and **2f** (white). Grid minima 1 and 2 are shown as light blue spheres. Compounds **2c** and **2f** exactly mapped both the minima, while **2d** and **2e** lose interactions with minimum 2 in order to map minimum 1.

For this purpose, available X-ray structures of reverse transcriptase bound to various NNRTIs were superimposed on the crystallographic complex RT:TNK-651 (1RT2)[17] and the *root-mean-square deviation* (rmsd) values for the residues forming the NNBP were calculated (see Supporting Information). Among the considered 44 RT:NNRTIs complexes, the crystallographic structures having the most different conformations of NNBP (chosen on the basis of rmsd value and visual inspection) with respect to 1RT2, were used to perform cross-docking simulations. The chosen X-ray structures were 1BQM, 1S9E, and 3HVT.[21−23] The performed cross-docking protocol confirmed that the initial conformation of the NNBP strongly influences the ligands' binding: in none of the first-ranked conformations did compounds **2c**−**f** show the "canonical" binding mode observed within the 1RT2 structure. The classical binding mode was, however, found at a higher energy level with respect to the first ranked conformation, and it was used as a starting point for the subsequent molecular dynamic simulations in order to evaluate the ability of the title compounds to reshape the NNBP.

The behavior of the most (**2c**) and least active (**2e**) compounds in the allosteric site of RT (wt) complexes was investigated by MD simulations in explicit solvent with the aim of observing

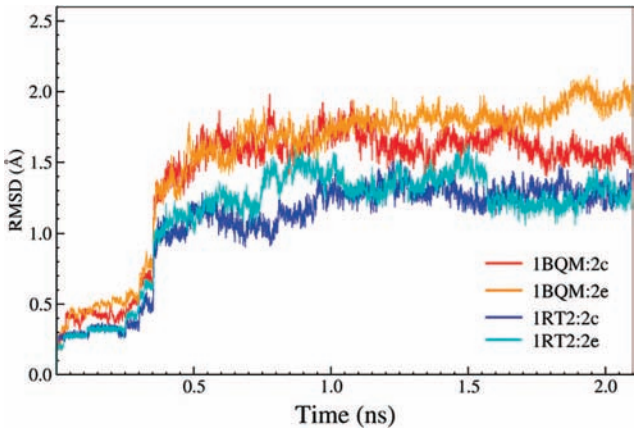


**Figure 5.** rmsd time evolution along the MD simulations.

the mutual rearrangement of both the ligands and the NNBP. It should be mentioned that, while the structure 1RT2 was cocrystallized with a compound (TNK-651) structurally similar to **2c** and **2e**, 1BQM was cocrystallized with inhibitor HBY 097, very dissimilar to **2c** and **2e**. As reported above, the best-scored docking solution of **2c**,**e** within the two crystals were not superimposable, but the docking procedure allowed us to select two similar geometries of the bound inhibitors as a reasonable starting point for the MD study (see above in the text "canonical binding mode"). Supramolecular assemblies were built by adding TIP3P water molecules and then they were submitted to a MD protocol. All heavy protein atoms were harmonically restrained with a force constant of 100 (kcal·mol$^{-1}$) Å$^2$ to the crystallographic position. Energy minimization followed by 0.250 ns of molecular dynamics under NPT (see Experimental Section, Molecular Dynamic Simulations) ensemble conditions were carried out. Subsequently, harmonic force constant was scaled by a factor of 10 every 50 ps and completely released after 100 ps of simulation. MD simulations were protracted for 1.6 ns. To describe the induced-fit properties of the ligands, the root-mean-square deviations (rmsd) of the atomic coordinates of the NNBP residues (see Experimental Section, Structure Preparation) were calculated for every frame of each MD simulation with respect to the starting point for that run. The rmsd values were used to quantify the drift of the NNBP structure from its initial conformation, therefore providing a crude measure of the "ligand's ability" to reshape the allosteric cavity (Figure 5).

As expected, the calculated rmsd for the NNBP of 1RT2 (blue and cyan lines in Figure 5) is less pronounced than that observed for the NNBP of 1BQM (orange and red lines in Figure 5) due to the similarity of **2c**,**e** with the 1RT2 cocrystallized ligand (TNK651). In fact, during the simulations, **2c**,**e** did not show any major rearrangement and did not induce a substantial remodeling of the allosteric site. On the contrary, both inhibitors in 1BQM showed a higher rmsd value. However, conversely to our expectations, the less active compound **2e** showed the highest rmsd trend (orange line in Figure 5), indicating a major rearrangement of the NNBP. To clarify these results, the protein−ligand and water−ligand average interaction energies were calculated over the last 200 ps of the MD simulations for all complexes and are reported in Table 3. In both crystallographic structures, **2c** showed the highest protein−ligand interaction energy (in absolute value) in agreement with the experimental activity data. Notably, we observed that the 1BQM:**2e** complex showed not only the lower protein−ligand interaction energy but also the highest water−ligand interaction energy in absolute value. These energies suggested that **2e** did not completely fit inside the NNBP of 1BQM and that it was more exposed to the solvent than **2c**. Therefore the observed highest rmsd value for the 1BQM:**2e** complex did not rely on the induced fit property of the ligand but reflected a sort of closure of the NNBP that was only partially occupied by the ligand.

The superposition of the first and the last minimized structures taken from the MD simulations of 1BQM and 1RT2 in complex with both **2c** and **2e** clearly shows what has been reported in Table 3 (Figure 6). In the case of 1BQM, the different behavior of **2c** versus **2e** can be clearly appreciated: while **2c** was able to fit into the allosteric site during the course of the dynamics simulation (Figure 6A), compound **2e** maintained substantially its starting pose and was unsuccessful in reshaping the allosteric cavity (Figure 6B). For comparison, the behavior of **2c**,**e** within the NNBP of 1RT2 is reported in Figure 6C,D: in this case, due to the structural similarity between the original ligand (TNK651) and **2c**,**e**, the first and last frame of the MD simulation are almost superimposable, no major reshaping of the allosteric cavity can be appreciated, and the inhibitors completely fit into the NNBP.

The energetic contribution of the only cyclopropyl moiety was also estimated in 1RT2:**2c** and 1RT2:**2e** in order to quantify its contribution to the total binding energy. A value of about 7−9% of the total protein−ligand interaction energy was found for both complexes (Table 3). Taken together, these results indicate that the right combination of chirality on C2 and C6 of the *S*-DABO scaffold is responsible for the high activity of compound **2c**, which, contrary to **2e**, seems to possess marked induced-fit properties that can be translated in the ability to reshape the NNBP in order to establish a more profitable interactions pattern (see MD movie in the Supporting Information).

In the attempt to rationalize the biological data on the K103N mutant (PDB entry 1IKY),[24] docking calculations highlighted again the importance of the C6′-(*R*)methyl group for the activity: while compounds **2c** and **2f** display a "canonical" binding mode inside the allosteric site, compounds **2d** and **2e** seem to bind the NNBP in a flipped conformation, with the 2,6-difluorophenyl ring in place of *p*-methoxyphenyl moiety and vice versa (Figure 7).

However, even if compound **2f** showed profitable interactions with the NNBP, a remarkable decrease of potency against the K103N mutant was found both in enzymatic and cellular assays. It is clear that the only discriminant between **2c** and **2f** is represented by the stereochemistry of the cyclopropyl moiety on the C2 chain, but, again, the docking studies on K103N were not able to find any major difference in the binding mode of these two compounds, which showed the same interaction pattern found for the parent compound **1** (Figure 7). As already reported by us,[8] the simple study of the interactions between ligand and protein does not seem to be sufficient to rationalize the biological data in the case K103N mutation, and other elements must be taken into account like the capacity of the molecules to disrupt the H-bond between Asn103 and Tyr188, allowing the opening and so the entrance into the NNBP. Unfortunately, molecular dynamics simulations conducted on compounds **2c**−**f** were not helpful in understanding this behavior. Accordingly, we decided to start a thorough kinetic study on both RT wild type and K103N mutant in order to get further information on the mechanism of action of **2c**−**f**, which could clarify the computational results.

**Kinetic Studies.** Kinetic parameters of the highly active compound **2c** were characterized toward RT (wt) using surface plasmon resonance (SPR) and compared to compound **1** and to

**Table 3.** rmsd Values for the Residues of the NNBP of 1RT2 and 1BQM from the Initial Minimized Structures Calculated in the Last 200 ps of MD[a]

| entry | X-ray | ligand | rms (Å) | protein−ligand (kcal·mol$^{-1}$) | water−ligand (kcal·mol$^{-1}$) | cyclopropyl−protein (kcal·mol$^{-1}$) |
|---|---|---|---|---|---|---|
| 1 | 1RT2 | **2c** (*R*,*R*,*R*) | 1.27 | −80.32 | −12.26 | −5.89 |
| 2 | 1RT2 | **2e** (*S*,*S*,*S*) | 1.28 | −76.36 | −15.54 | −6.57 |
| 3 | 1BQM | **2c** (*R*,*R*,*R*) | 1.56 | −78.21 | −16.42 | |
| 4 | 1BQM | **2e** (*S*,*S*,*S*) | 1.96 | −63.57 | −25.01 | |

[a] Protein−ligand, water−ligand, and ligand cyclopropane moiety−protein interaction energies, calculated in the last 200 ps of MD, are kcal·mol$^{-1}$.

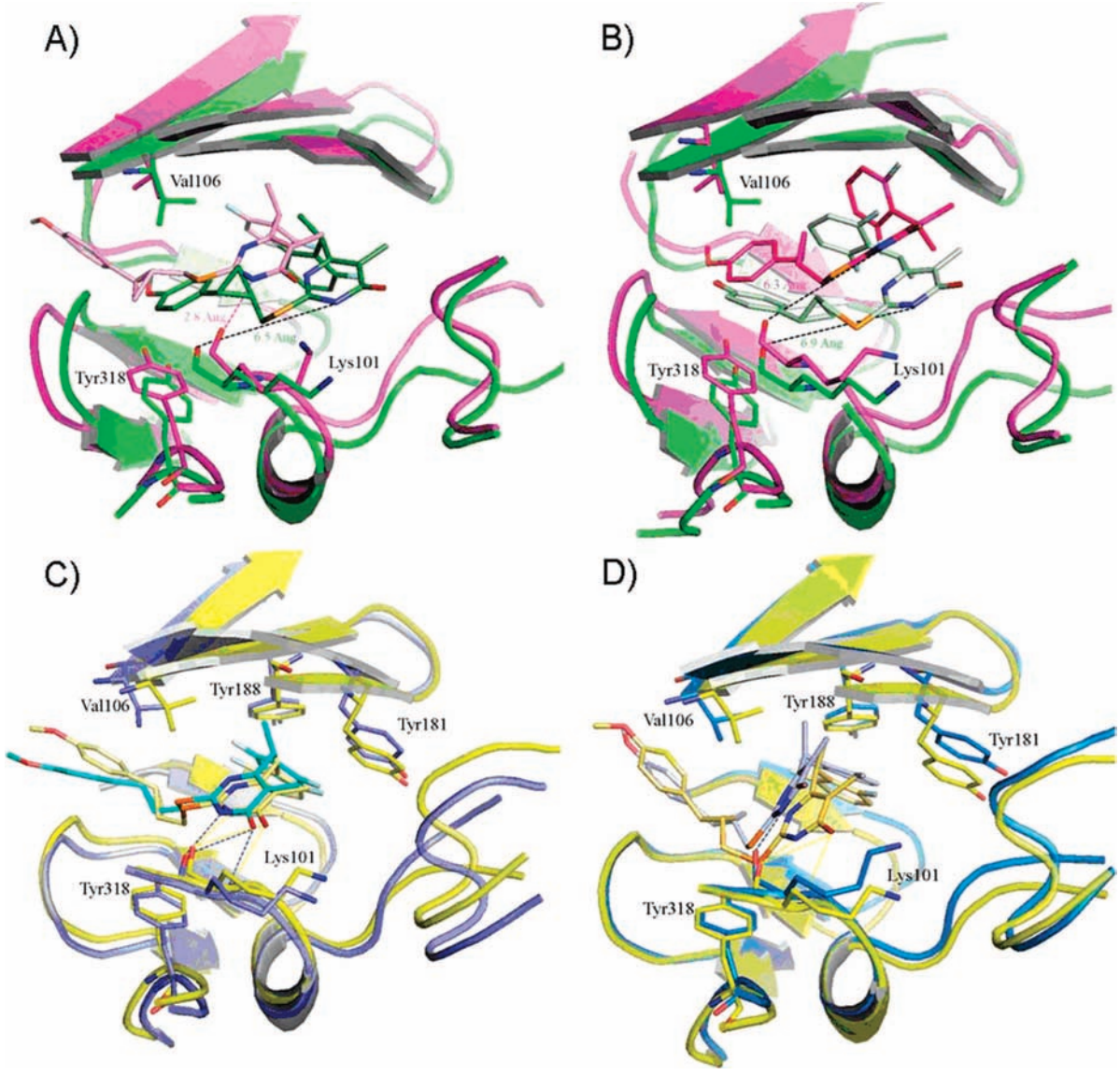


**Figure 6.** (A) Superposition of first (green) and last (purple/pink) minimized frames coming from dynamic simulations of 1BQM:**2c**. (B) Superposition of first (green/white) and last (purple/pink) minimized frames of 1BQM:**2e**. (C) Superposition of first (yellow) and last (blue/cyan) minimized frames of 1RT2:**2c**. (D) Superposition of first (yellow) and last (blue/cyan) minimized frames of 1RT2:**2e**. In (A) and (B), the distances between amidic N atom of pyrimidinone ring and the carbonylic C atom of Lys101 are reported as black dashed lines. Notably, only compound **2c** is able to form the typical H bond (shown as purple line in A) with the backbone of Lys101. In (C) and (D), the hydrogen bonds are reported as yellow (for the first minimized frame) or blue (for the last frame) dashed lines.

the recently approved anti-HIV drug Etravirine (TMC125)[25] used as a reference of high-affinity compound. Our results show that all the inhibitors dissociate very slowly if at all from a RT surface (Figure 8) as shown by similar flat curves (at time >2400 s) and cannot be quantitatively differentiated by SPR. These observations further confirm the results of our MD studies: as can be clearly appreciated from the movie in the Supporting Information, during the course of the dynamics simulation, the most active compound **2c** is deeply incorporated within the NNBP, which, at the end, completely surround the inhibitor.

Data analysis revealed that compound **2c** binds very tightly to the RT with an apparent association rate constant $k_a = (1.0 \pm 0.4)10^4$ M$^{-1}$ s$^{-1}$ and a dissociation rate constant $k_d = (2.1 \pm 3.5)10^{-5}$ s$^{-1}$ (beyond the measurable limit of the instrument). Kinetic parameters evaluated for **1** were $k_a = 1 \times 10^4$ M$^{-1}$s$^{-1}$ and $k_d \leq 6 \times 10^{-5}$ s$^{-1}$, and those for TMC125 were $k_a = 0.8 \times 10^4$ M$^{-1}$s$^{-1}$ and $k_d \leq 4 \times 10^{-5}$ s$^{-1}$. These data reveal the small dissociation rates for the three compounds and are significantly lower than values obtained by the same technique for Delavirdine, Efavirenz, and Nevirapine, which range from

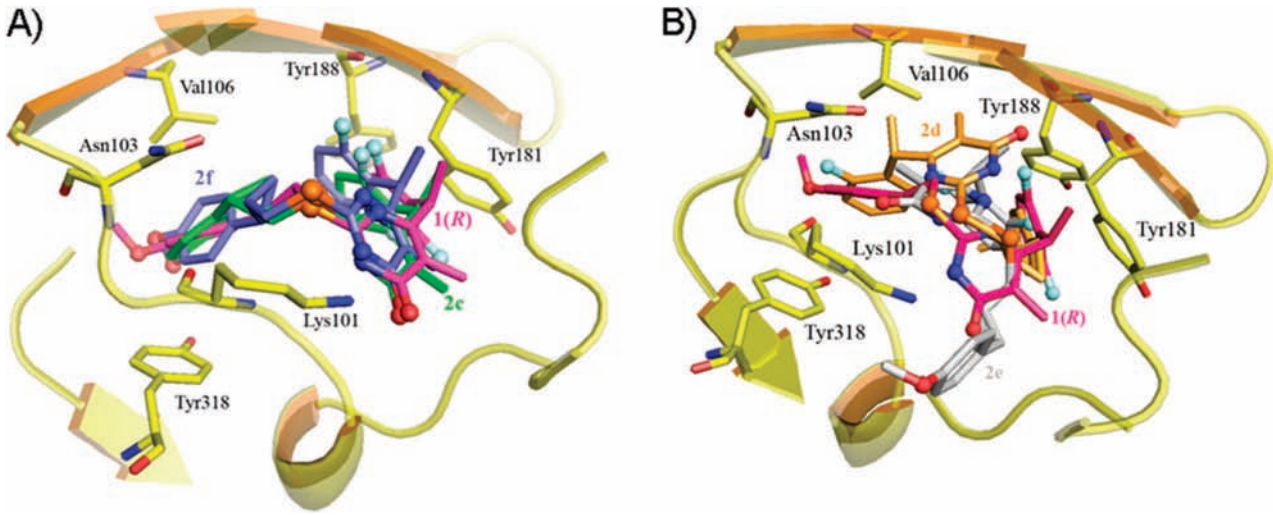


**Figure 7.** (A) Binding mode of compounds **2c** (reported in ball and stick and colored in green), **2f** (ball and stick, blue), and **1**(*R*) (ball and stick, purple) into K103N NNBP (PDB entry 1IKY). (B) Binding mode of **2d** (ball and stick, orange), **2e** (ball and stick, light gray), and **1**(*R*) (ball and stick, purple) into K103N NNBP (PDB entry 1IKY).

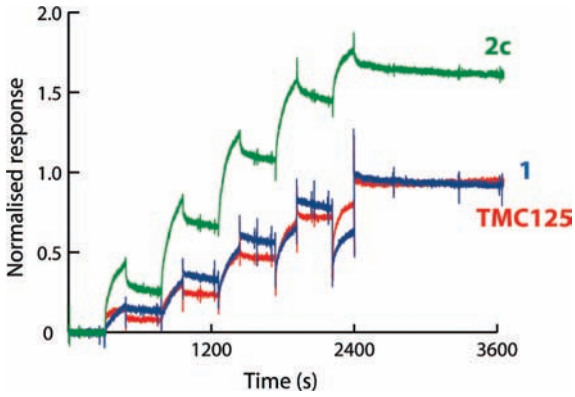


**Figure 8.** Kinetic titrations of RT interactions with compounds **2c**, **1**, and TMC125. The three sensorgrams were obtained in independent experiments. The scale for the SPR response signal was normalized assuming a 1:1 binding stoichiometry. Original responses ranged between 0 and 70 RU for **2c** (green line) and 0−40 RU for **1** (blue line) and TMC125 (red line). A 2-fold increase in sample concentration was used for each compound during successive injections (0.075, 0.15, 0.3, 0.6, and 1.2 $\mu$M).

$1 \times 10^{-2}$ to $2 \times 10^{-3}$ $s^{-1}$.[26] It can also be appreciated that, at saturating amount of inhibitor **2c** ($\geq$1.2 $\mu$M), the signal was observed to exceed the maximum for a 1:1 interaction and this could be due to (i) the presence of two binding sites for **2c** on RT or (ii) a slow conformational alteration induced by the binding of the inhibitor.[27]

While the interaction of **2c** with two different binding sites on RT cannot be either confirmed or excluded with the data at present in our hands, the pronounced induced-fit properties of **2c**, found with the MD simulations herein reported, suggest that the conformational alteration of RT could be a possible explanation for the atypical binding stoichiometry.

Finally, to determine the mode of action of compound **2c**, the dependence of the inhibition on both the nucleic acid (NA) and the nucleotide substrate (dNTP) was studied. The kinetic parameters $K_m$ and $V_{max}$ were calculated at increasing concentration of the inhibitor **2c** and compared to the values obtained in the absence of the inhibitor. As shown in Figure 9, in the presence of **2c**, no significant variations were noted in the $K_m$ values for both substrates (Figure 9A,B), while the $V_{max}$ was reduced in a dose-dependent manner (Figure 9C). Similar results were obtained for the other diasteroisomers **2d**−**f** (data not shown). These results showed that **2c** is a noncompetitive inhibitor of HIV-1 RT wt. The same experiments were repeated in the presence of the HIV-1 RT K103N mutant. As shown in Figure 9D, the $K_m$ values for the nucleic acid substrate were significantly decreased by increasing concentrations of **2c**, whereas the corresponding values for the nucleotide substrate were unaffected (Figure 9E). The $V_{max}$ values were decreased, as expected (Figure 9F). Similar results were obtained for the other diasteroisomers **2d**−**f** (data not shown).

By analyzing the variation of the apparent $K_m$ and $V_{max}$ values as a function of the inhibitor concentrations, it was possible to determine the equilibrium dissociation constants ($K_i$) for the three enzymatic forms along the reaction pathway, namely the free enzyme (E), the binary complex with the nucleic acid (E:NA), and the ternary complex with both substrates (E:NA:dNTP). In addition, equilibrium binding studies were applied to derive the respective association ($k_{on}$) and dissociation ($k_{off}$) rates. The corresponding values are listed in Table 4. These results indicated that compounds **2c**−**f** are mixed-type inhibitors of HIV-1 RT K103N, with a more preferential association to the enzyme−substrate complex than to the free RT. These findings further support an induce-fit mechanism of action for these compounds and can justify the failure of our molecular modeling approach to rationalize the activity of compounds **2c**−**f** because all the calculations were performed on the free enzyme and, unfortunately, no crystal structure of the K103N in the binary or ternary complex is at present available to repeat the calculations. In the end, by comparing the $K_i$ for the ternary complex of the wild type and K103N enzymes, it appeared that compound **2c** showed only a 3.3-fold reduction in its inhibition potency due to the mutation. In comparison, the clinically used NNRTIs Efavirenz and Nevirapine showed a loss of potency of 50- and 10- fold, respectively. As a result, **2c** was 6- fold more potent than Efavirenz and 125-fold more potent than Nevirapine against the K103N mutant.

## Conclusions

In the present study, the role played by the stereochemistry on the C2-substituent (left part) of the *S*-DABO analogues for anti-HIV-1 activity was investigated for the first time. The introduction of different stereocenters on important pharmacophoric site of a promising RT-inhibitor such as **1** could also

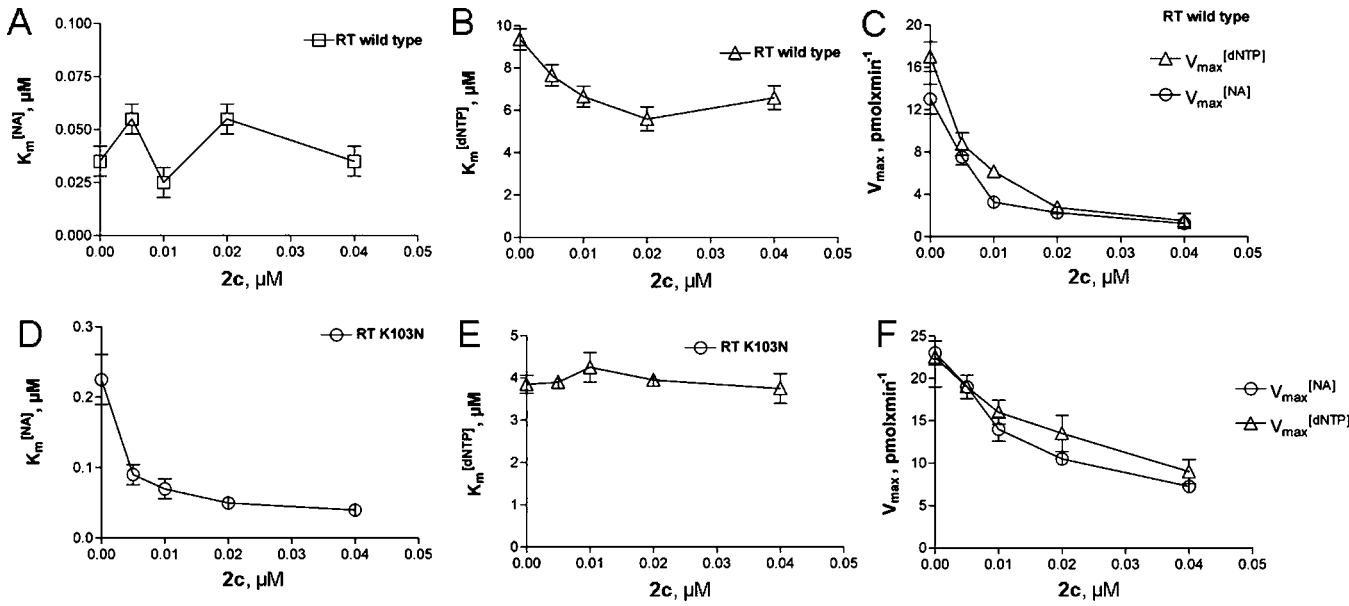


**Figure 9.** (A) Variation of the apparent affinity of RT wt for the nucleic acid ($K_m^{[NA]}$) as a function of the inhibitor **2c** concentration. (B) Variation of the apparent affinity of RT wt for the nucleotide substrate ($K_m^{[dNTP]}$) as a function of the inhibitor **2c** concentration. (C) Variation of the $V_{max}$ of the reaction with RT wt obtained varying the nucleic acid (circles) or the nucleotide (triangles) substrates as a function of the inhibitor **2c** concentration. (D−F) The same as in (A−C), but in the presence of the K103N mutant RT. The $K_m$ and $V_{max}$ values were determined as described in the Experimental Section. Values are the mean of three independent estimates. Error bars represent ± SD.

**Table 4.** Kinetics of the Binding of **2c** and **2f** to RT (wt) and K103N

| | E | | | E:DNA | | | E:DNA:dNTP | | |
|---|---|---|---|---|---|---|---|---|---|
| compd | $K_i$[a] μM | $k_{on}$ $M^{-1}$ $s^{-1}$ × $10^4$ | $k_{off}$ $s^{-1}$ × $10^{-4}$ | $K_i$ μM | $k_{on}$ $M^{-1}$ $s^{-1}$ × $10^4$ | $k_{off}$ $s^{-1}$ × $10^{-4}$ | $K_i$ μM | $k_{on}$ $M^{-1}$ $s^{-1}$ × $10^4$ | $k_{off}$ $s^{-1}$ × $10^{-4}$ |
| | | | | HIV-1 RT Wild Type | | | | | |
| **2c** | 0.01 (±0.002) | 0.8 (±0.1) | 8 (±1) | 0.008 (±0.001) | 1.5 (±0.2) | 1.3 (±1) | 0.009 (±0.001) | 4.1 (±0.3) | 4 (±0.5) |
| **2f** | 0.04 (±0.005) | 1.2 (±0.1) | 5 (±0.5) | 0.03 (±0.004) | 1.3 (±0.1) | 5 (±0.5) | 0.04 (±0.003) | 1.2 (±0.1) | 5 (±0.5) |
| EFZ | 0.03 (±0.008) | 1 (±0.1) | 3 (±0.3) | 0.03 (±0.007) | 1 (±0.1) | 3 (±0.3) | 0.004 (±0.001) | 4 (±0.2) | 1.6 (±0.2) |
| NVP | 0.4 (±0.06) | 0.4 (±0.1) | 16 (±1) | 0.5 (±0.1) | 0.3 (±0.02) | 15 (±0.01) | 0.4 (±0.08) | 0.4 (±0.1) | 16 (±1) |
| | | | | HIV-1 RT K103N | | | | | |
| **2c** | 0.065 (±0.005) | 1.2 (±0.2) | 8 (±1) | 0.04 (±0.003) | 1.3 (±0.2) | 5 (±0.5) | 0.03 (±0.003) | 1.5 (±0.1) | 5 (±0.5) |
| **2f** | 0.6 (±0.01) | 0.1 (±0.02) | 6 (±0.7) | 0.4 (±0.05) | 0.1 (±0.02) | 4 (±0.4) | 0.3 (±0.04) | 0.1 (±0.02) | 3 (±0.3) |
| EFZ | 1.5 (±0.2) | 2 (±0.3) | 30 (±3) | 1.6 (±0.2) | 2.5 (±0.3) | 40 (±5) | 0.2 (±0.01) | 6 (±1) | 12 (±1) |
| NVP | 4 (±0.2) | 0.04 (±0.005) | 16 (±1) | 4 (±0.2) | 0.04 ±0.005) | 16 (±2) | 5 (±0.5) | 0.03 (±0.005) | 15 (±2) |

[a] E, free Enzyme; E:NA, binary complex of the enzyme and the nucleic acid (NA); E:NA:dNTP, ternary complex of the enzyme, the nucleic acid, and the nucleotide substrate (dNTP).

allow us to generate a collection of enantiopure drugs with improved activity and potential usefulness in overcoming future drug-induced mutation. Accordingly, the C2-cyclopropyl analogue (**2**) of compound **1** was synthesized and its four diastereoisomers obtained via semipreparative HPLC. Results from enzymatic and cellular assays revealed the importance of the right combination of the stereochemistry on the left (C2-substituent) and right part (C6-substituent) of the *S*-DABO scaffold for the inhibition of both wild type and drug resistant enzymes, particularly the K103N mutant. The (*R*,*R*) configuration of the cyclopropane ring in C2, coupled with a C6′-(*R*)methyl group gave the promising lead compound **2c**, which exhibited picomolar activity against RT (wt) and nanomolar activity against all the tested mutants. A computational protocol comprising docking studies, grid mapping, cross-docking experiments, and dynamics simulation was successfully applied for the rationalization of the biological results on wild type RT. However, the same approach failed when applied to the K103N mutant, possibly because of a preferential association of **2c**−**f** to the enzyme−substrate complex as indicated by a thorough kinetic enzymatic study. Real-time binding kinetics of our inhibitors was characterized using surface plasmon resonance (SPR), revealing that compound **2c** has a similar behavior to the recently approved anti-HIV drugs Etravirine (TMC125), with an extremely low dissociation constant. These data confirm the results of our MD studies which show that the lead compound **2c** is more effective in reshaping the allosteric cavity, which, at the end, completely surrounds the inhibitor. The SPR study also revealed that, at saturating amount of inhibitor **2c** (≥1.2 μM), the signal was observed to exceed the maximum for a 1:1 interaction; further studies are ongoing in order to completely exclude the interaction of **2c** with two different binding sites on RT (wt).

## Experimental Section

**General Considerations.** Reagents were obtained from commercial suppliers and used without further purifications. According

to standard procedures, $CH_2Cl_2$ was dried over calcium hydride and DMF was bought already anhydrous. Anhydrous reactions were run under a positive pressure of dry $N_2$ or argon. IR spectra were recorded on a Perkin-Elmer BX FT-IR system using $CHCl_3$ as the solvent. TLC was carried out using Merck TLC plates Kieselgel 60 $F_{254}$. Chromatographic purifications were performed on columns packed with Merck 60 silica gel, 23−400 mesh, for flash technique. Melting points were measured using a Gallenkamp melting point apparatus and are uncorrected. $^1$H NMR spectra were recorded with a Bruker AC200F spectrometer at 200 MHz, and chemical shifts are reported in values relative to TMS at 0.00 ppm. $CDCl_3$ was used as solvent. Optical rotations have been measured on a Perkin-Elmer 343 polarimeter equipped with a sodium lamp ($\lambda = 589$ nm) and a 10 cm microcell.

**HPLC and MS Analysis.** Mass spectral (MS) data were obtained using an Agilent 1100 LC/MSD VL system (G1946C) with a 0.4 mL/min flow rate using a binary solvent system of 95:5 MeOH/water and an electrospray ionization source (ESI). UV detection was monitored at 254 nm. Mass spectra were acquired in positive mode scanning over the mass range of 50−1500. The following ion source parameters were used: drying gas flow, 9 mL·min$^{-1}$; nebulizer pressure, 40 psi; drying gas temperature, 350 °C.

The purity of compound *rac*-**2** was assessed by HPLC (Agilent 1100 LC/MSD VL system (G1946C)) using a Zorbax Eclipse XDB, 4.6 mm × 150 mm, 5 $\mu$m C8 column with a mobile phase composed of MeOH/$H_2O$ (80:20) at a flow rate of 1 mL·min$^{-1}$ (all solvents were HPLC grade, Fluka).

Enantiomeric excess of (R,R)-**5** and (S,S)-**5** was established with a Varian ProStar HPLC system (Varian Analytical Instruments, Perkin-Elmer Inc. USA equipped with a binary pump with manual injection valve and model ProStar 325 UV−vis detector) using a Chiralcel OD 0.46 cm × 25 cm column, with a mobile phase composed of hexane/iPrOH, 95:5 at a flow rate of 0.8 mL·min$^{-1}$.

The two diastereoisomeric mixtures **2a** and **2b** were resolved on a Varian ProStar HPLC system using a semipreparative Alltima C18 250 mm × 10 mm column with a mobile phase composed of $CH_3CN$/formic acid 0.1% 70:30 at a flow rate of 2.5 mL·min$^{-1}$.

Diasteromeric excess of **2c**−**f** was established by reinjecting every single compound in the semipreparative Alltima C18 250 mm × 10 mm column with a mobile phase composed of $CH_3CN$/formic acid 0.1% 70:30 at a flow rate of 2.5 mL·min$^{-1}$ (Varian ProStar HPLC system).

The enantiomeric mixture *rac*-**1** was resolved on a Varian ProStar HPLC system using a semipreparative CHIRALPAK A, 250 mm × 10 mm column with a mobile phase composed of hexane/iPrOH, 80/20, at a flow rate of 2.5 mL/min.

**Microwave Irradiation Experiments.** Microwave reactions were conducted using a CEM Discover Synthesis Unit (CEM Corp., Matthews, NC). The machine consists of a continuous focused microwave-power delivery system with operator-selectable power output from 0 to 300 W. The temperature of the contents of the vessel was monitored using a calibrated infrared temperature control mounted under the reaction vessel. All experiments were performed using a stirring option whereby the contents of the vessel are stirred by means of a rotating magnetic plate located below the floor of the microwave cavity and a Teflon-coated magnetic stir bar in the vessel.

**Molecular Docking Studies.** All calculations and manipulations were performed following a previously reported protocol.[8] The geometry of each inhibitor was optimized using the ab initio quantum chemistry program GAUSSIAN[28] and the HF/6-31G* basis set, in order to calculate partial atomic charges. Consequently, a set of atom-centered RHF HF/6-31G* charges was obtained for each inhibitor, by application of RESP methodology.[29]

**GRID-Based Binding Site Analysis.** Computation of Molecular Interaction Fields (MIFs) over the NNBP was carried out with software GRID, version 22.[18] Box dimensions were defined so as to accommodate all the residues constituting the NNBP and the NPLA (Number of Planes of grid points per Å) parameter was set to 3. A value of 3 was used for the GRID keyword NPLA, which is the number of planes of GRID points per Å and determines the resolution of the computation: the GRID points were 0.333 Å apart. A value of 0 was used for the GRID keyword MOVE, thus allowing lone pairs and tautomeric hydrogen atoms to move in response to the probe. To achieve the points of minimum of molecular interaction fields (MIFs), Grid calculations were performed using the export GRIDKONT option. The *kont* file was then processed by means of the *minim* and *filmap* programs (both implemented in the Grid package) that extract all the points of minimum of MIF and retain only those falling under a user-defined cutoff, fixed to 0 kcal·mol$^{-1}$. The result of this procedure is a file with a .pdb extension containing the 3D coordinates of the points of minimum of the interaction energy, together with the corresponding energy values.

**Structure Preparation.** Forty-four X-ray crystal structures of RT complexed with a NNRTI were retrieved from the Protein Data Bank (Table S1, Supporting Information). For the cross-docking studies, complexes were prepared as previously reported[8] and backbone atoms of each crystal structure were superimposed with RT/TNK-651 PDB entry 1RT2)[17] as reference. The superposition of the RT complexes was performed with the program Pymol version 0.99 using the implemented Shindyalov and Bourne algorithm.[30,31] The rmsd values for all residues backbone atoms and of heavy atoms of residues (forming the NNBP) Pro95A, Leu100A-Lys103A, Val106A, Val179A-Tyr181A, Tyr188A-Gly190A, Phe227A, Trp229A, Leu234A-Pro236A, and Tyr318A were calculated and are reported in Table S1, Supporting Information. The complexes with the highest rmsd values (arbitrarily chosen over 1.85 Å and reported in bold in Table S1, Supporting Information) were subjected to visual inspection. Complexes with PDB codes 1TV6, 2B5J, and 2BE2[32,33] were discarded since the peculiar orientation of the aromatic side chain of Tyr181 that points away from the polymerase active site as in the apo-RT structure. Among X-ray structures 1S6P, 1S9G, 1S9E, and 1SUQ, which show very similar NNBP, 1S9E was chosen as representative complex for subsequent calculations. So, complexes 1BQM, 1S9E, and 3HVT were used to perform cross-docking calculations, applying the same protocol previously described.[8]

**Molecular Dynamics Simulations.** Atom types, covalent and nonbonded parameters were assigned to inhibitors from those already present in the AMBER force field, by analogy or through interpolation.[34] Charges were calculated as previously described (see Molecular Docking Studies). System setup, molecular dynamics (MD), and postdynamic analysis were performed with NAMD2 (v2.6)[35] and VMD (v1.8.6)[36] software packages. Supramolecular assemblies to be subjected to MD studies were built starting from appropriate AutoDock output complexes (see docking section). Each complex were surrounded by a periodic box of TIP3P water molecules[37] that extended about 9.0 A from the protein atoms and 12 $Cl^-$ ions were added to conserve neutrality of the system. For each system, the number of water molecules was 30170 and the initial dimensions of the rectangular periodic box were about 120 × 87 × 115 Å. The simulations were conducted using periodic boundary conditions (PBC) and particle mesh Ewald (PME) method[38] with grid size of 100 × 80 × 100 Å. The nonbonded cutoff was set to 10.0 Å, the switching distance to 9 Å and the nonbonded pair list distance to 14 Å. The r-RESPA multiple time step method[39] was employed with 1 fs for bonded, 2 fs short-range for nonbonded, and 4 fs for long-range electrostatic forces. Hydrogen atoms were free to move. Molecules were simulated for a total of 2.1 ns in the NPT ensemble. The temperature was set to 310 K and controlled via Langevin thermostat with a dumping factor of 5 ps$^{-1}$. The pressure of 1 atm was controlled via isotropic Langevin piston barostat with oscillation period of 200 fs, damping time scale of 100 fs, and noise temperature of 310 K. At this stage, water molecules, ligand and hydrogen atoms were free to move, while heavy protein atoms were restrained to the crystallographic position using a value of 4 in the harmonic energy function exponent and with constant of force of 100.0 kcal·mol$^{-1}$ Å$^{-1}$. The starting assemblies were relaxed with 2000 steps of conjugate gradient energy minimization to remove unfavorable contacts. The obtained structures were then subjected to 250 ps of MD with same harmonic

restraints and same constant of force. Subsequently, harmonic force constant were scaled by a factor of 10 every 50 ps and they were completely released after 100 ps of dynamic simulation. Random velocities were reassigned according to the temperature system every 50 ps over the first 0.5 ns of the simulation with the purpose to enhance disruption in the NNBP. MD simulations were protracted for 1.6 ns in the NPT ensemble and trajectories were stored each 400 fs.

**Biological Evaluation. Expression, Purification, and Cloning of Recombinant HIV-1 RT Forms.** Recombinant heterodimeric RT, either wild type or the K103N variant, were expressed and purified as briefly described below. The HIV-1 RT gene fragment spanning codons 2 to 261 from pHXB2D2-261RT constructs carrying the K103N mutation was amplified by PCR, digested with Acc1 and Pvu2, and cloned into the expression plasmid p6HRT (ΔXho1/Bgl2), containing the wild type RT gene. The resulting p6HRT expression vectors with the K103N mutation were used for the production in *E. coli* (BL21) and purification of recombinant His-tagged RT enzymes in a fast protein liquid chromatography (F-PLC) system, using Ni-NTA superflow column (QIAGEN, USA) (Abdullah, N.; Chase, H. A. *Biotechnol. Bioeng.* **2005**, *92*, 501–513). All the enzymes were purified to a >95% purity, as confirmed by sodium dodecyl sulfate-polyacrylamide gel electrophoresis and Gelcode Blue stain, and had a specific activity on poly(rA):oligo(dT). One Unit of DNA polymerase activity corresponds to the incorporation of 1 nmol of dNMP into acid-precipitable material in 60 min at 37 °C.Western Blotting confirmed the identity of the polypeptides present in the final preparation with anti-RT monoclonal antibodies.

**HIV-1 RT RNA-Dependent DNA Polymerase Activity Assay.** Poly(rA)/oligo(dT) was used as a template for the RNA-dependent DNA polymerase reaction by HIV-1 RT, either wt or carrying the mutations. For the activity assay, a 25 $\mu$L final reaction volume contained TDB buffer (50 mM Tris-HCl (pH 8.0), 1 mM dithiothreitol (DTT), 0.2 mg/mL bovine serum albumin (BSA), 2% glycerol), 10 mM $MgCl_2$, 0.5 mg of poly(rA):oligo$(dT)_{10:1}$ (0.3 mM 3′ −OH ends), 10 mM [$^3$H]dTTP 1 Ci·mmol$^{-1}$ and, finally, introduced into tubes containing aliquots of different enzyme concentrations (5−10 nM RT). After incubation at 37 °C for indicated time, 20 $\mu$L from each reaction tube were spiked on glass fiber filters GF/C and immediately immersed in 5% ice-cold trichloroacetic acid (TCA) (AppliChem GmbH, Darmstadt). Filters were washed three times with 5% TCA and once with ethanol for 5 min, then dried and, finally, added with EcoLume Scintillation cocktail (ICN, Research Products Division, Costa Mesa, CA), to detect the acid-precipitable radioactivity by PerkinElmer Trilux MicroBeta 1450 Counter.

**Anti-HIV Activity in Lymphoid Cells.** Biological activity of the compounds was tested in the lymphoid MT-4 cell line (received from the NIH AIDS Reagent Program) against the wt HIV-1 NL4-3 strain and three different HIV-1 strains, as described before.[40] Briefly, MT-4 cells were infected with the appropriate HIV-1 strain (or mock-infected to determine cytotoxicity) in the presence of different drug concentrations. At day five postinfection, a tetrazolium-based colorimetric method (MTT method) was used to evaluate the number of viable cells. The HIV-1 strains containing the multi-NNRTI mutation, K103N or the Y188L mutant, were received from the Medical Research Council Centralised Facility for AIDS Reagents, Herfordshire, UK.

**Kinetic Analysis.** The mechanism of action of the compounds was found to be either fully noncompetitive or partially mixed. According to the ordered mechanism of the polymerization reaction, whereby template-primer (TP) binds first followed by the addition of dNTP, HIV-1 RT can be present in three different catalytic forms: as a free enzyme, in a binary complex with the nucleic acid (NA), and in a ternary complex with NA and dNTP. The resulting rate equation for such a system is very complex and impractical to use. For these reasons, the general steady-state kinetic analysis was simplified by varying one of the substrates (either NA or dNTP) while the other was kept constant. When the NA substrate was held constant at saturating concentration and the inhibition at various concentrations of dNTPs was analyzed, at the steady-state, all of the input RT was in the form of the RT/NA binary complex and only two forms of the enzyme (the binary complex and the ternary complex with dNTP) could react with the inhibitor. Similarly, when the dNTP concentration was kept constant at saturating levels and the inhibition at various NA concentrations was analyzed, RT was present either as a free enzyme or in the ternary complex with NA and dNTP. The steady-state rate equation used for the partially mixed inhibition was the one describing a reaction involving only two mechanistic forms of the enzyme:

$$v = \{[V_{max}/(1 + I/K''_i)]/[1 + (K_m/S)] \cdot [(1 + I/K'_i)/(1 + I/(K''_i)\} \quad (1)$$

When NA was saturating, $K'_i = K_i^{free}$, whereas at saturating dNTP $K'_i = K_i^{bin}$. In all cases, $K''_i = K_i^{ter}$. According to the mixed-type mechanism of eq (1), it follows that, if $K'_i > K''_i$, then both $K_m$ and $V_{max}$ values will decrease at increasing inhibitor concentrations. When $K'_i = K''_i$, then the eq (1) can be simplified to the one describing a fully noncompetitive mechanism.

The equilibrium dissociation constants ($K'_i$ and $K''_i$) were calculated from the variations of the $K_m$ and $V_{max}$ values as a function of the inhibitor concentrations according to the equations:

$$K'_i = I/\{[K_p(1 + I/K'_i)/K_m] - 1\} \quad (2)$$

$$K''_i = I/[(V_{max}/V_p) - 1] \quad (3)$$

where $K_p$ and $V_p$ are the apparent $K_m$ and $V_{max}$ values, respectively, at each given inhibitor concentration.

Kinetics of inhibitor binding experiments were as described previously. Briefly, HIV-1 RT (20−40 nM) was incubated for 2 min at 37 °C in a final volume of 4 $\mu$L in the presence of TDB buffer, with 10 mM $MgCl_2$ alone or with 100 nM 3′-OH ends (for the formation of the RT/TP complex), or in the same mixture complemented with 10 $\mu$M unlabeled dTTP (for the formation of the RT/TP/dNTP complex). The inhibitor to be tested was then added to a final volume of 5 $\mu$L at a concentration at which [EI]/[E0] = [1 − 1/(1 + [I]/$K_i$)] > 0.9. Then, 145 $\mu$L of a mix containing TDB buffer, 10 mM $MgCl_2$, and 10 $\mu$M [$^3$H]dTTP (5 Ci/mmol) was added at different time points. After an additional 10 min of incubation at 37 °C, 50 $\mu$L aliquots were spotted on GF/C filters and acid-precipitable radioactivity was measured as described for the HIV-1 RT RNA-dependent DNA polymerase activity assay. The $v_t/v_0$ ratio, representing the normalized difference between the amount of dTTP incorporated at the zero time point and at different time points, was then plotted against time.

The apparent binding rate ($k_{app}$) values were determined by fitting the experimental data to the single-exponential equation:

$$vt/v0 = e^{-k}app^{t(4)} \quad (4)$$

where $t$ is time. If $[E]_0$ is the input enzyme concentration, $[E]_t$ is the enzyme available for the reaction at time $t$, and $[E:I]_t$ is the enzyme bound to the inhibitor at time $t$, it follows that

$$[E]_t = [E]_0 - [E:I]_t \quad (5)$$

Because $v_0 = k_{cat}[E]_0$ and $v_t = k_{cat}[E]_t$, then $v_t/v_0 = 1 - [E:I]_t/[E]_0$. Thus, the $v_t/v_0$ value is proportional to the fraction of enzyme bound to the inhibitor.

The true association ($k_{on}$) and dissociation ($k_{off}$) rates were calculated from the equations:

$$k_{app} = k_{on}([I] + K_i) \quad (6)$$

$$k_{off} = k_{on}K_i \quad (7)$$

Data analysis and statistics: Data obtained were analyzed by nonlinear regression analysis using GraphPad Software (San Diego, CA).

**Surface Plasmon Resonance.** The interactions between HIV-1 RT and inhibitors were studied using a BIAcore 2000 instrument (GE Healthcare). Interaction between a protein immobilized on a

biosensor chip and a compound flowed over the surface was monitored in real time as a change in surface plasmon resonance units. CM5 sensor chips (research grade) were used for the experiments. For immobilization, HIV-RT sensor surfaces were prepared using the amine coupling chemistry as described in refs 26 and 27. Final immobilization levels were between 10000 and 12500 resonance units (RU), corresponding to approximately 10 to 12.5 ng of reverse transcriptase·$mm^{-2}$. A dextran surface treated in the same way but without protein injection was used as a reference.

Kinetic titration experiments were performed at 25 °C using 10 mM Hepes, 150 mM NaCl, 3.4 mM EDTA, 0,01% surfactant P20 (polysorbate Tween-20), 4% DMSO, pH 7.5 as running buffer. The inhibitor was serially diluted in running buffer to working concentrations. Within a single binding cycle, the samples were injected sequentially in order of increasing concentration over both the reference and RT protein surfaces. Also, prior to and after the binding cycle, buffer was injected for ≪blank≫ responses essential to double-reference the data.

Compounds **1**, **2c**, or TMC-125 were injected sequentially for 3 min at a flow rate of 50 $\mu L \cdot min^{-1}$ over the reference and reverse transcriptase surfaces. At the end of each injection, the dissociation phase was set to 2 min. Data were also collected during the washing steps, providing a total of 4.5 min of dissociation-phase information for each injection. The final dissociation phase after the last injection of the cycle lasted for 20 min.

For data processing, data were double-referenced by subtracting both the data obtained from the reference surface, and the buffer response on the protein surface to remove systematic noise and instrument drift. Data recorded during the injection phase were not corrected for DMSO solvent effect. For easy comparison between data sets, all experiments were normalized by dividing the response (RU) by the theoretical $R_{max}$ value, corresponding to the amount of protein immobilized for each inhibitor cycle. The data were fitted with the software BIAevaluation assuming a simple 1:1 association model (see Supporting Information).

Because of the observed extremely slow off-rates of the compounds and the impossibility to correctly regenerate the surface after a first experiment, the interaction was analyzed using the kinetic titration method described in Karlsson and colleagues[41] and for which the evaluation model was recently made available commercially. This method is particularly adapted in the case where the complex is very stable, making it difficult to identify regeneration conditions that dissociate the complex while keeping the immobilized protein active. It allows the determination of the kinetics parameters as accurately as the classical multi steps analysis.

**X-ray Crystallography.** X-ray diffraction data were collected on a single crystal of **2d** using a Siemens P4 four-circle diffractometer with graphite monochromated Mo Kα radiation ($\lambda$ = 0.71073 Å). The structure was solved by direct methods implemented in the SHELXS-97 program.[42] The refinement was carried out by full-matrix anisotropic least-squares on $F^2$ for all reflections for non-H atoms by using the SHELXL-97 program.[43]

**Acknowledgment.** This study was supported by grants from the European THiNC and ExCellENT-HIT Consortiums. The University of Siena and the Spanish BFU2006-00966 and FIS PI060624 are also acknowledged for financial support. S.Z. is the recipient of a Buzzati-Traverso Fellowship. This work was also supported by grants from the French National Agency for AIDS Research (ANRS) (to E.E.). The following reagent was obtained through the NIH AIDS Research and Reference Reagent Program, Division AIDS, NIAID, NIH: TMC-125 (Etravirine), catalogue no. 11609, from Tibotec Pharmaceuticals, Inc. Prof. Gabriele Cruciani (University of Perugia, Italy) is also acknowledged for kindly providing us with the GRID program.

**Supporting Information Available:** Details of synthesis and analytical data, additional molecular modeling information and a movie of the MD simulation for compounds **2e** (left side) and **2c** (right side) within the NNBP of 1BQM (AVI). This material is available free of charge via the Internet at http://pubs.acs.org.

## References

(1) Greenea, W. C.; Debyserb, Z.; Ikedac, Y.; Freedd, E. O.; Stephense, E.; Yonemotoa, W.; Buckheitf, R. W.; Esté, J. A.; Cihlarh, T. Novel targets for HIV therapy. *Antivir. Res.* **2008**, in press.

(2) (a) Este, J. A.; Telenti, A. HIV entry inhibitors. *Lancet* **2007**, *370*, 81–88. (b) Fatkenheuer, G.; Pozniak, A. L.; Johnson, M. A.; Plettenberg, A.; Staszewski, S.; Hoepelman, A. I.; Saag, M. S.; Goebel, F. D.; Rockstroh, J. K.; Dezube, B. J.; Jenkins, T. M.; Medhurst, C.; Sullivan, J. F.; Ridgway, C.; Abel, S.; James, I. T.; Youle, M.; van der Ryst, E. Efficacy of short-term monotherapy with maraviroc, a new CCR5 antagonist, in patients infected with HIV-1. *Nat. Med.* **2005**, *11*, 1170–1172.

(3) (a) Markowitz, M.; Nguyen, B. Y.; Gotuzzo, E.; Mendo, F.; Ratanasuwan, W.; Kovacs, C.; Prada, G.;, Morales-Ramirez, J. O.; Crumpacker, C. S.; Isaacs, R. D., Gilde, L. R.; Wan, H.; Miller, M. D.; Wenning, L. A.; Teppler, H. Rapid and Durable Antiretroviral Effect of the HIV-1 Integrase Inhibitor Raltegravir as Part of Combination Therapy in Treatment-Naive Patients With HIV-1 Infection: Results of a 48-Week Controlled Study. *JAIDS, J. Acquir. Immune Defic. Syndr.* **2007**, *46*, 125−133. (b) Saag, M.; Ive, P.; Heera, J.; Tawadrous, M.; DeJesus, E.; Clumeck, N.; Cooper, D.; Horban, A.; Mohapi, L.; Mingrone, H.; Reyes-Teran, G.; Walmsley, S.; Hackman, F.; van der Ryst, E.; Mayer, H. 4th International AIDS Society Conference on HIV Pathogenesis, Treatment and Prevention, Sydney, Australia, 2007; WESS104.

(4) Ren, J.; Stammers, D. K. Structural basis for drug resistance mechanisms for non-nucleoside inhibitors of HIV reverse transcriptase. *Virus Res.* **2008**, *134*, 157–170.

(5) (a) Boone, L. R. Next-generation HIV-1 non-nucleoside reverse transcriptase inhibitors. *Curr. Opin. Invest. Drugs* **2006**, *7*, 128–135. (b) Barbaro, G.; Scozzafava, A.; Mastrolorenzo, A.; Supuran, C. T. Highly Active Antiretroviral Therapy: Current State of the Art, New Agents and Their Pharmacological Interactions Useful for Improving Therapeutic Outcome. *Curr. Pharm. Des.* **2005**, *11*, 1805–1843.

(6) (a) Brito, M. A.; Rodrigues, C. R.; Cirino, J. J. V.; de Alencastro, R. B.; Castro, H. C.; Albuquerque, M. G. 3D-QSAR CoMFA of a Series of DABO Derivatives as HIV-1 Reverse Transcriptase Non-Nucleoside Inhibitors. *J. Chem. Inf. Model.* **2008**, *48*, 1706–1715. (b) Barreiro, G.; Guimaraes, C. R. W.; Tubert-Brohman, I.; Lyons, T. M.; Tirado-Rives, J.; Jorgensen, W. L. Search for Non-Nucleoside Inhibitors of HIV-1 Reverse Transcriptase Using Chemical Similarity, Molecular Docking, and MM-GB/SA Scoring. *J. Chem. Inf. Model.* **2007**, *47*, 2416–2428. (c) Mai, A.; Artico, M.; Rotili, D.; Tarantino, D.; Clotet-Codina, I.; Armand-Ugon, M.; Ragno, R.; Simeoni, S.; Sbardella, G.; Nawrozkij, M. B.; Samuele, A.; Maga, G.; Este, J. A. Synthesis and biological properties of novel 2-aminopyrimidin-4(3*H*)-ones highly potent against HIV-1 mutant strains. *J. Med. Chem.* **2007**, *50*, 5412–5424. (d) Mai, A.; Sbardella, G.; Artico, M.; Ragno, R.; Massa, S.; Novellino, E.; Greco, G.; Lavecchia, A.; Musiu, C.; La Colla, M.; Murgioni, C.; La Colla, P.; Loddo, R. Structure-based design, synthesis, and biological evaluation of conformationally restricted novel 2-alkylthio-6-[1-(2,6-difluorophenyl)alkyl]-3,4-dihydro-5-alkylpyrimidin-4(3*H*)-ones as non-nucleoside inhibitors of HIV-1 reverse transcriptase. *J. Med. Chem.* **2001**, *44*, 2544–2554.

(7) (a) Manetti, F.; Este, J. A.; Clotet-Codina, I.; Armand-Ugon, M.; Maga, G.; Crespan, E.; Cancio, R.; Mugnaini, C.; Bernardini, C.; Togninelli, A.; Carmi, C.; Alongi, M.; Petricci, E.; Massa, S.; Corelli, F.; Botta, M. Parallel solution-phase and microwave-assisted synthesis of new *S*-DABO derivatives endowed with subnanomolar anti-HIV-1 activity. *J. Med. Chem.* **2005**, *48*, 8000–8008. (b) Botta, M.; Corelli, F.; Petricci, E.; Radi, M.; Maga, G.; Esté, J. A.; Mai, A. Patent WO 2007/043094 A2, 2007.

(8) Mugnaini, C.; Alongi, M.; Togninelli, A.; Gevariya, H.; Brizzi, A.; Manetti, F.; Bernardini, C.; Angeli, L.; Tafi, A.; Bellucci, L.; Corelli, F.; Massa, S.; Maga, G.; Samuele, A.; Facchini, M.; Clotet-Codina, I.; Armand-Ugón, M.; Esté, J. A.; Botta, M. Dihydro-alkylthio-benzyl-oxopyrimidines as inhibitors of reverse transcriptase: synthesis and rationalization of the biological data on both wild-type enzyme and relevant clinical mutants. *J. Med. Chem.* **2007**, *50*, 6580–6595.

(9) Nawrozkij, M. B.; Rotili, D.; Tarantino, D.; Botta, G.; Eremiychuk, A. S.; Musmuca, I.; Ragno, R.; Samuele, A.; Zanoli, S.; Armand-Ugón, M.; Clotet-Codina, I.; Novakov, I. A.; Orlinson, B. S.; Maga, G.; Esté, J. A.; Artico, M.; Mai, A. 5-Alkyl-6-benzyl-2-(2-*oxo*-2-phenylethylsulfanyl)pyrimidin-4(3*H*)-ones, a series of anti-HIV-1 agents of the dihydro-alkoxy-benzyl-oxopyrimidine family with peculiar structure−activity relationship profile. *J. Med. Chem.* **2008**, *51*, 4641–4652.

(10) Beroza, P.; Suto, M. J. Designing chiral libraries for drug discovery. *Drug Discovery Today* **2000**, *5*, 364–372.
(11) Quaglia, M. G.; Mai, A.; Sbardella, G.; Artico, M.; Ragno, R.; Massa, S.; Del Piano, D.; Setzu, G.; Dorattiotto, S.; Cotichini, V. Chiral resolution and molecular modeling investigation of *rac*-2-cyclopentylthio-6-[1-(2,6-difluorophenyl)ethyl]-3,4-dihydro-5-methylpyrimidin-4(3*H*)-one (MC-1047), a potent anti-HIV-1 reverse transcriptase agent of the DABO class. *Chirality* **2001**, *13*, 75–80.
(12) Denmark, S. E.; James, E. A. A comparison of (chloromethyl)- and (iodomethyl)zinc cyclopropanation reagents. *J. Org. Chem.* **1991**, *56*, 6974–6981.
(13) (a) Denmark, S. E.; O'Connor, S. P. Catalytic, Enantioselective Cyclopropanation of Allylic Alcohols. Substrate Generality. *J. Org. Chem.* **1997**, *62*, 584–594. (b) Denmark, S. E.; O'Connor, S. P. Enantioselective Cyclopropanation of Allylic Alcohols. The Effect of Zinc Iodide. *J. Org. Chem.* **1997**, *62*, 3390–3401.
(14) $C_{24}H_{24}F_2N_2O_2S$, Mr 442.52, crystal dimensions: 0.6 mm × 0.5 mm × 0.3 mm, Triclinic, *P*1, $a = 9.744(5)$Å, $b = 15.490(2)$ Å, $c = 15.970(1)$ Å, $\alpha = 71.863(5)°$, $\beta = 83.636(17)°$, $\gamma = 87.130(14)°$, $Z = 4$, $\rho_{calcd} = 1.291$ g cm$^{-3}$, graphite monochromated Mo Kα radiation ($\lambda = 0.71073$ Å), $\mu$ (Mo-Kα) $= 0.181$ mm$^{-1}$, $T = 293(2)$ K, $2\theta_{max} = 50.0°$, 8400 measured reflections with $R_{int} = 0.001$, $R = 0.0680$ and w$R = 0.1430$ for all reflections, last $\Delta\rho$ map of −0.29 and 0.39 eÅ$^{-3}$. The crystallographic data of the structure have been deposited at the Cambridge Crystallographic Data Centre with deposit number CCDC 695593. These data can be obtained free of charge via www.ccdc-.cam.ac.uk/conts/retrieving.html (or from the Cambridge Crystallographic Data Centre, 12 Union Road, Cambridge CB2 1EZ, UK; fax: (+44) 1223−336−033; or e-mail: deposit@ccdc.cam.ac.uk).
(15) Data not shown.
(16) Morris, G. M.; Goodsell, D. S.; Halliday, R. S.; Huey, R.; Hart, W. E.; Belew, R. K.; Olson, A. J. Automated Docking Using a Lamarckian Genetic Algorithm and and Empirical Binding Free Energy Function. *J. Comput. Chem.* **1998**, *19*, 1639–1662.
(17) Hopkins, A. L.; Ren, J.; Esnouf, R. M.; Willcox, B. E.; Jones, E. Y.; Ross, C.; Miyasaka, T.; Walker, R. T.; Tanaka, H.; Stammers, D. K.; Stuart, D. I. Complexes of HIV-1 reverse transcriptase with inhibitors of the HEPT series reveal conformational changes relevant to the design of potent non-nucleoside inhibitors. *J. Med. Chem.* **1996**, *39*, 1589–1600.
(18) *Grid, version 22*; Molecular Discovery, Ltd: Marsh Road, Pinner, Middlesex, UK, 2004.
(19) Ragno, R.; Frasca, S.; Manetti, F.; Brizzi, A.; Massa, S. Docking and 3-D QSAR Studies on Indolyl Aryl Sulfones. Binding Mode Exploration at the HIHIV-Reverse Transcriptase Inhibition: Inclusion of Ligand-Induced Fit by Cross-Docking Studies. *J. Med. Chem.* **2005**, *48*, 200–212.
(20) Kroeger Smith, M. B.; Rouzer, C. A.; Taneyhill, L. A.; Smith, N. A.; Hughes, S. H.; Boyer, P. L.; Janssen, P. A.; Moereels, H.; Koymans, L.; Arnold, E.; Ding, J.; Das, K.; Zhang, W.; Michejda, C. J.; Smith, R. H., Jr. Molecular modeling studies of HIV-1 reverse transcriptase nonnucleoside inhibitors: total energy of complexation as a predictor of drug placement and activity. *Protein Sci.* **1995**, *4*, 2203–2222.
(21) Hsiou, Y.; Das, K.; Ding, J.; Clark, A. D., Jr.; Kleim, J. P.; Rosner, M.; Winkler, I.; Riess, G.; Hughes, S. H.; Arnold, E. Structures of Tyr188Leu mutant and wild-type HIV-1 reverse transcriptase complexed with the non-nucleoside inhibitor HBY 097: inhibitor flexibility is a useful design feature for reducing drug resistance. *J. Mol. Biol.* **1998**, *284*, 313–323.
(22) Das, K.; Clark, A. D.; Lewi, P. J.; Heeres, J.; De Jonge, M. R.; Koymans, L. M.; Vinkers, H. M.; Daeyaert, F.; Ludovici, D. W.; Kukla, M. J.; De Corte, B.; Kavash, R. W.; Ho, C. Y.; Ye, H.; Lichtenstein, M. A.; Andries, K.; Pauwels, R.; Boyer, P. L.; Clark, P.; Hughes, S. H.; Janssen, P. A.; Arnold, E. Roles of Conformational and Positional Adaptability in Structure-Based Design of TMC125-R165335 (Etravirine) and Related Non-nucleoside Reverse Transcriptase Inhibitors That Are Highly Potent and Effective against Wild-Type and Drug-Resistant HIV-1 Variants. *J. Med. Chem.* **2004**, *47*, 2550–2560.
(23) Wang, J.; Smerdon, S. J.; Jager, J.; Kohlstaedt, L. A.; Rice, P. A.; Friedman, J. M.; Steitz, T. A. Structural basis of asymmetry in the human immunodeficiency virus type 1 reverse transcriptase heterodimer. *Proc. Natl. Acad. Sci. U.S.A.* **1994**, *91*, 7242–7246.
(24) Lindberg, J.; Sigurdsson, S.; Lowgren, S.; Andersson, H. O.; Sahlberg, C.; Noreen, R.; Fridborg, K.; Zhang, H.; Unge, T. Structural basis for the inhibitory efficacy of efavirenz (DMP-266), MSC194 and PNU142721 towards the HIV-1 RT K103N mutant. *Eur. J. Biochem.* **2002**, *269*, 1670–1677.
(25) Ludovici, D. W.; De Corte, B. L.; Kukla, M. J.; Ye, H.; Ho, C. Y.; Lichtenstein, M. A.; Kavash, R. W.; Andries, K.; de Bethune, M. P.; Azijn, H.; Pauwels, R.; Lewi, P. J.; Heeres, J.; Koymans, L. M. H.; de Jonge, M. R.; Van Aken, K. J. A.; Daeyaert, F. F. D.; Das, K.; Arnold, E.; Janssen, P. A. J. Evolution of anti-HIV drug candidates. Part 3: diarylpyrimidine (DAPY) analogues. *Bioorg. Med. Chem. Lett.* **2001**, *11*, 2235–2239.
(26) Geitmann, M.; Unge, T.; Danielson, U. H. Interaction Kinetic Characterization of HIV-1 Reverse Transcriptase Non-nucleoside Inhibitor Resistance. *J. Med. Chem.* **2006**, *49*, 2375–2387.
(27) Geitmann, M.; Unge, T.; Danielson, U. H. Biosensor-Based Kinetic Characterization of the Interaction between HIV-1 Reverse Transcriptase and Non-nucleoside Inhibitors. *J. Med. Chem.* **2006**, *49*, 2367–2374.
(28) Frisch, M. J. ; Trucks, G. W.; Schlegel, H. B.; Scusera, G. E.; Robb, M. A.; Cheeseman, J. R.; Zakrzewski, V. G.; . Montgomery, J. A., Jr.; Stratmann, R. E., Burant, J. C.; Dapprich, S.; Millam, J. M.; Daniels, A. D.; Kudin, K. N.; Strain, M. C.; Farkas, O.; Tomasi, J.; Barone, V.; Cossi, M.; Cammi, R.; Mennucci, B.; Pomelli, C.; Adamo, C.; Clifford, S.; Ochterski, J.; Petersson, G. A.; Ayala, P. Y.; Cui, Q.; Morokuma, K.; Malick, D. K.; Rabuck, A. D.; Raghavachari, K.; Foresman, J. B.; Cioslowski, J.; Ortiz, J. V.; Stefanov, B. B.; Liu, G.; Liashenko, A.; Piskorz, P.; Komaromi, I.; Gomperts, R.; Martin, R. L.; Fox, D. J.; Keith, T.; Al-Laham, M. A.; Peng, C. Y.; Nanayakkara, A.; Gonzalez, C.; Challacombe, M.; Gill, P. M. W.; Johnson, B. G.; Chen, W.; Wong, M. W.; Andres, J. L.; Gonzale, C.; Head-Gordon, M.; Replogle, E. S.; Pople, J. A. *Gaussian 98, evision A.11.2*; Gaussian, Inc.; Pittsburgh, PA, 2001.
(29) Bayly, C. I.; Cieplak, P.; Cornell, W. D.; Kollman, P. A. A well-behaved electrostatic potential based method using charge restraints for deriving atomic charges: the RESP model. *J. Phys. Chem.* **1993**, *97*, 10269–80.
(30) DeLano, W. L. *The PyMOL Molecular Graphics System*; DeLano Scientific LLC: San Carlos, CA, 2002; http://www.pymol.org.
(31) Shindyalov, N.; Bourne, P. E. Protein structure aligment by incremental combinatorial extension (CE) of the optimal path. *Protein Eng.* **1998**, *11*, 739–747.
(32) Pata, J. D.; Stirtan, W. G.; Goldstein, S. W.; Steitz, T. A. Structure of HIV-1 reverse transcriptase bound to an inhibitor active against mutant RTs resistant to other non-nucleoside inhibitors. *Proc. Natl. Acad. Sci. U.S.A.* **2004**, *101*, 10548–10553.
(33) Himmel, D. M.; Das, K., Jr.; Hughes, S. H.; Benjahad, A.; Oumouch, S.; Guillemont, J.; Coupa, S.; Poncelet, A.; Csoka, I.; Meyer, C.; Andries, K.; Nguyen, C. H.; Grierson, D. S.; Arnold, E. Crystal Structures for HIV-1 Reverse Transcriptase in Complexes with Three Pyridinone Derivatives: A New Class of Non-Nucleoside Inhibitors Effective against a Broad Range of Drug-Resistant Strains. *J. Med. Chem.* **2005**, *48*, 7582–7591.
(34) Cornell, W. D.; Cieplak, P.; Bayly, C. I.; Gould, I. R.; MerzJr., K. M.; Ferguson, D. M.; Spellmeyer, D. C.; Fox, T.; Caldwell, J. W.; Kollman, P. A. A Second Generation Force Field for the Simulation of Proteins, Nucleic Acids, and Organic Molecules. *J. Am. Chem. Soc.* **1995**, *117*, 5179–51977.
(35) Phillips, J. C.; Braun, R.; Wang, W.; Gumbart, J.; Tajkhorshid, E.; Villa, E.; Chipot, C.; Skeel, R. D.; Kale, L.; Schulten, K. Scalable molecular dynamics with NAMD. *J. Comput. Chem.* **2005**, *26*, 1781–1802.
(36) Humphrey, W.; Dalke, A.; Schulten, K. VMD−Visual Molecular Dynamics. *J. Mol. Graphics* **1996**, *14*, 33–38.
(37) Jorgensen, W. L.; Chandrasekhar, J.; Madura, J. D.; Impey, R. W.; Klein, M. L. Comparison of simple potential functions for simulating liquid water. *J. Chem. Phys.* **1983**, *79*, 926–935.
(38) Essman, U.; Perera, L.; Berkowitz, M. L.; Darden, T.; Lee, H.; Pedersen, L. A smooth particle mesh Ewald method. *J. Chem. Phys.* **1995**, *103*, 8577–8593.
(39) Tuckerman, M.; Berne, B.; Martyna, G. Reversible multiple time scale molecular dynamics. *J. Chem. Phys.* **1992**, *97*, 1990–2001.
(40) Armand-Ugon, M.; Gutierrez, A.; Clotet, B.; Este, J. A. HIV-1 Resistance to the gp41-Dependent Fusion Inhibitor C-34. *Antiviral Res.* **2003**, *59*, 137–142.
(41) Karlsson, R.; Katsamba, P. S.; Nordin, H.; Pol, E.; Myszka, D. G. Analyzing a kinetic titration series using affinity biosensors. *Anal. Biochem.* **2006**, *349*, 136–147.
(42) Sheldrick, G. M., *SHELXS-97, Release 97−2, Program for the Solution of Crystal Structures*; University of Göttingen: Göttingen, Germany, 1997.
(43) Sheldrick G. M. *SHELXL-97, Release 97−2, Program for Crystal Structure Refinement*; University of Göttingen: Göttingen, Germany, 1997.

JM801330N